Wiley Series on Electrocatalysis and Electrochemistry

Andrzej Wieckowski, Series Editor

VIBRATIONAL SPECTROSCOPY AT ELECTRIFIED INTERFACES

Edited by Andrzej Wieckowski, Carol Korzeniewski and Björn Braunschweig

With a Foreword by Masatoshi Osawa, Hokkaido University

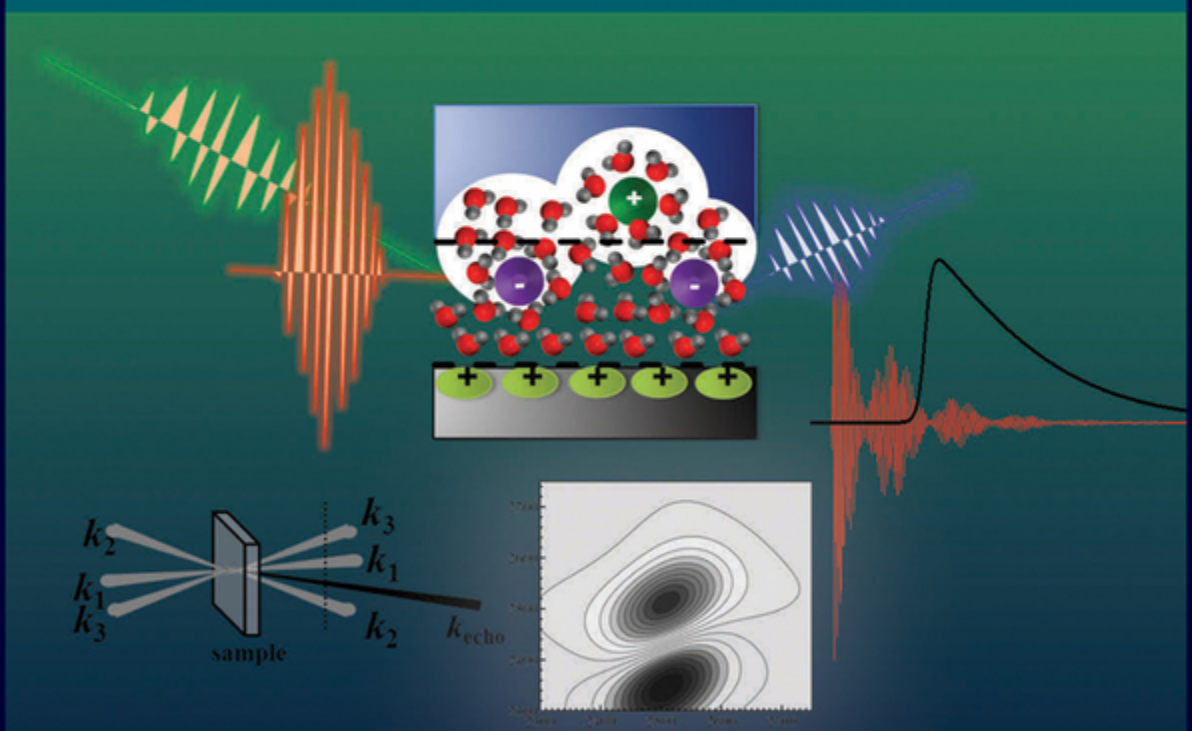

WILEY

Vibrational Spectroscopy at Electrified Interfaces

WILEY SERIES ON ELECTROCATALYSIS AND ELECTROCHEMISTRY

Andrzej Wieckowski, Series Editor

Synthetic Diamond Films: Preparation, Electrochemistry, Characterization and Applications, Edited by Enric Brillas and Carlos Alberto Martínez-Huitle

Fuel Cell Catalysis: A Surface Science Approach, Edited by Marc T. M. Koper

Electrochemistry of Functional Supramolecular Systems, Margherita Venturi, Paola Ceroni, And Alberto Credi

Catalysis in Electrochemistry: From Fundamentals to Strategies for Fuel Cell Development, Elizabeth Santos and Wolfgang Schmickler

Fuel Cell Science: Theory, Fundamentals, and Biocatalysis, Andrzej Wieckowski and Jens Norskov

Vibrational Spectroscopy at Electrified Interfaces

Edited by

Andrzej Wieckowski
Carol Korzeniewski
Björn Braunschweig

Wiley Series on Electrocatalysis and Electrochemistry

WILEY

Published by John Wiley & Sons, Inc., Hoboken, New Jersey
Published simultaneously in Canada

Library of Congress Cataloging-in-Publication Data is available.
9781118157176

Printed in the United States of America

10 9 8 7 6 5 4 3 2 1

Contents

Preface to the Wiley Series on Electrocatalysis and Electrochemistry

This series covers recent advances in electrocatalysis and electrochemistry and depicts prospects for their contribution into the present and future of the industrial world. It aims to illustrate the transition of electrochemical sciences from its beginnings as a solid chapter of physical chemistry (covering mainly electron transfer reactions, concepts of electrode potentials, and structure of electrical double layer) to the field in which electrochemical reactivity is shown as a unique chapter of heterogeneous catalysis, is supported by high-level theory, connects to other areas of science, and includes focus on electrode surface structure, reaction environment, and interfacial spectroscopy.

The scope of this series ranges from electrocatalysis (practice, theory, relevance to fuel cell science and technology) to electrochemical charge transfer reactions, biocatalysis, and photoelectrochemistry. While individual volumes may appear quite diverse, the series promises updated and overall synergistic reports providing insights to help further our understanding of the properties of electrified solid–liquid systems. Readers of the series will also find strong reference to theoretical approaches for predicting electrocatalytic reactivity by such high-level theories as density functional theory. Beyond the theoretical perspective, further vehicles for growth are such significant topics such as energy storage, syntheses of catalytic materials via rational design, nanometer-scale technologies, prospects in electrosynthesis, new instrumentation, and surface modifications. In this context, the reader will notice that new methods being developed for one field may be readily adapted for application in another.

Electrochemistry and electrocatalysis have both benefited from numerous monographs and review articles due to their depth, complexity, and relevance to the practical world. The Wiley Series on Electrocatalysis and Electrochemistry is dedicated to present the current activity by focusing each volume on a specific topic that is timely and promising in terms of its potential toward useful science and technology. The chapters in these volumes will also demonstrate the connection of electrochemistry to other disciplines beyond chemistry and chemical engineering, such as physics, quantum mechanics, surface science, and biology. The integral goal is to offer a broad-based analysis of the total development of the fields. The progress of the series will provide a global definition of what electrocatalysis and electrochemistry are now, and will contain projections about how these fields will further evolve in time. The purpose is twofold, to provide a modern reference for graduate instruction and for active researchers in the two disciplines, as well as to document that

electrocatalysis and electrochemistry are dynamic fields that are expanding rapidly, and are likewise rapidly changing in their scientific profiles and potential.

Creation of each volume required the editors involvement, vision, enthusiasm, and time. The Series Editor thanks each Volume Editor who graciously accepted his invitation. Special thanks go to Ms. Anita Lekhwani, the Series Acquisitions Editor, who extended the invitation to edit this series to me and has been a wonderful help in its assembling process.

ANDRZEJ WIECKOWSKI
Series Editor

Foreword

Despite extensive efforts, the electrochemical interface, where central processes in electrochemical reactions occur, had long been a black box until researchers started to shed light on it in the 1960s. At the beginning, the light used was mostly that in the visible region, but information obtainable by visible light was very limited, and the use of vibrational spectroscopy, which can provide detailed information on molecules, was strongly desired. In 1974, an innovation was made in spectroelectrochemistry by the application of Raman spectroscopy. It is well known that the Raman study of pyridine adsorbed on silver electrodes led to the discovery of surface-enhanced Raman scattering (SERS). The application of infrared reflection absorption spectroscopy (IRAS) to electrochemical interfaces in 1980 also was a great achievement. Surface-enhanced infrared absorption (SEIRA), an effect similar to SERS, was discovered in the same year, and the first observation of sum frequency generation (SFG) from monolayers on solid surfaces was made in 1986, although their applications to electrochemical interfaces were somewhat delayed. During the last four decades, these surface vibrational spectroscopy techniques have been advanced greatly owing to the improvement in instrumentation and the development of experimental techniques, which are still further developing year by year.

Vibrational spectroscopy is a powerful tool to identify molecules and to study their structures and reactions, as it is often mentioned that *vibrational spectra are letters from molecules*. It is also the case at surfaces and interfaces. It provides us information on adsorbed structures and orientations of molecules. Spectra are sensitive to changes in the environment at interfaces, from which we can obtain deeper insight into chemistry and physics at the interfaces. In situ, time-resolved monitoring of reactions taking place at surfaces and interfaces is also possible. Owing to these advantages, they have gained wide application, from fundamental electrochemistry to many other related fields of science and technology, including surface science, heterogeneous electrocatalysis, energy conversion, biochemistry, nanotechnology, and sensors. However, each technique has strong and weak points. Difficulty in interpretation of the obtained spectra is another problem. For appropriate use of the techniques and for correct interpretation of spectra, sufficient fundamental understanding of the techniques is required.

This book, which features all the aforementioned four surface vibrational spectroscopy techniques and their applications to recent research topics, will provide fundamental information for nonspecialists and an up-to-date account of recent advances in this field for specialists.

Masatoshi Osawa
Catalysis Research Center, Hokkaido University, Sapporo, Japan

Preface

Electrified interfaces play an important role in many phenomena. Electric fields that develop at junctions between different phases can align molecules and ions into configurations that greatly influence the physical and chemical nature of the interface. The molecular structure of charged interfaces impacts many practical processes, including energy conversion in batteries, solar cells, and fuel cells, corrosion at solid surfaces, chemical reactions over oxide particles in the earth and atmosphere, biochemical transformations, signal transduction in chemical sensors, and heterogeneous catalytic reactions, to name a few.

Surface vibrational spectroscopy techniques probe the structure and composition of interfaces at a molecular level. Their versatility and typically nondestructive nature often enable in situ measurements of operating devices and monitoring of interface-controlled processes under reactive conditions. This book highlights modern applications of Raman, infrared, and nonlinear optical spectroscopy in the study of charged interfaces.

Early chapters in the book provide a glimpse into the breadth of systems that can be investigated through the use of nonlinear optical techniques. Properties of interfacial water, ions, and biomolecules at charged dielectric, metal oxide, and electronically conductive metal catalyst surfaces, as probed by nonlinear optical techniques, are discussed in Part I. In addition to examples of practical experimental interest, the chapters guide readers to the latest in measurement and instrumental techniques. Part II includes coverage of Raman spectroscopy from the standpoint of sensitive approaches for detection of biomolecules at solid–liquid interfaces and the use of photon depolarization strategies to elucidate molecular orientation at surfaces. Part III reports on wide-ranging systems from small fuel molecules at well-defined surfaces to macromolecular complexes as building blocks of functional interfaces in devices that have applications in chemical sensing and electric power generation. These interfaces are amenable for infrared spectroscopy due to versatile sampling methods, that is, specular and diffuse reflectance, polarization–modulation, and total internal reflection modes.

Andrzej Wieckowski
Carol Korzeniewski
Björn Braunschweig

Contributors

Christopher M. Berg
School of Chemical Sciences
University of Illinois
Urbana, Illinois

Björn Braunschweig
Institute of Particle Technology (LFG)
Erlangen, Germany

Christa L. Brosseau
Department of Chemistry
Saint Mary's University, Halifax
Nova Scotia, Canada

Angel Cuesta
Instituto de Química Física
"Rocasolano"
CSIC
Madrid, Spain

Dana D. Dlott
School of Chemical Sciences
University of Illinois
Urbana, Illinois

Jonathan Doan
Department of Chemistry and Chemical Biology
Northeastern University
Boston, Massachusetts

Kathrin Engelhardt
Institute of Particle Technology (LFG)
Erlangen, Germany

Michael D. Fayer
Department of Chemistry
Stanford University
Stanford, California

Juan M. Feliu
Instituto de Electroquímica
Universidad de Alicante
Alicante, Spain

Emily E. Fenn
Department of Chemistry
Stanford University
Stanford, California

Ian Kendrick
Department of Chemistry and Chemical Biology
Northeastern University
Boston, Massachusetts

Carol Korzeniewski
Department of Chemistry
Texas Tech University
Lubbock, Texas

Agata Królikowska
Department of Chemistry
Warsaw University
Warsaw, Poland

Robert B. Kutz
Champaign, Illinois

Annia H. Kycia
Department of Chemistry
University of Guelph,
Guelph, Ontario, Canada

Jacek Lipkowski
Department of Chemistry
University of Guelph
Guelph, Ontario, Canada

Prabuddha Mukherjee
Urbana, Illinois

Kei Murakoshi
Department of Chemistry
Faculty of Science
Hokkaido University
Sapporo, Japan

Hideki Nabika
Department of Material and Biological Chemistry, Faculty of Science
Yamagata University
Yamagata, Japan

Fumika Nagasawa
Department of Chemistry
Faculty of Science
Hokkaido University
Sapporo, Japan

José Manuel Orts
Instituto de Electroquímica
Universidad de Alicante
Alicante, Spain

Wolfgang Peukert
Institute of Particle Technology (LFG)
Erlangen, Germany

Duc Thanh Pham
Institute of Physical Chemistry
University of Bonn
Bonn, Germany

Antonio Rodes
Instituto de Electroquímica
Universidad de Alicante
Alicante, Spain

Melanie Röefzaad
Institute of Physical and Theoretical Chemistry
University of Bonn
Bonn, Germany

Armin Rumpel
SwissOptic AG
Heerbrugg, Switzerland

Andrea P. Sandoval
Departamento de Quimica, Facultad de Ciencias
Universidad Nacional de Colombia
Bogotá, Colombia

Y. Ron Shen
Physics Department
University of California, Berkeley
Berkeley, California

Eugene S. Smotkin
Department of Chemistry and Chemical Biology
Northeastern University
Boston, Massachusetts

ZhangFei Su
Department of Chemistry
University of Guelph
Guelph, Ontario, Canada

Mai Takase
Catalysis Research Center
Hokkaido University
Sapporo, Japan

Klaus Wandelt
Institute of Physical and Theortetical Chemistry
University of Bonn
Bonn, Germany, and
Institute of Experimental Physics
University of Wroclaw
Wroclaw, Poland

Glenn A. Waychunas
Geochemistry Department
Earth Sciences Division
Lawrence Berkeley National Laboratory
Berkeley, California

Andrzej Wieckowski
Department of Chemistry
University of Illinois at Urbana Champaign
Urbana, Illinois

Part One

Nonlinear Vibrational Spectroscopy

Chapter 1

Water Hydrogen Bonding Dynamics at Charged Interfaces Observed with Ultrafast Nonlinear Vibrational Spectroscopy

Emily E. Fenn and Michael D. Fayer
Department of Chemistry, Stanford University, Stanford, California

1.1 INTRODUCTION

The question of how charged species affect water structure and dynamics is relevant to many applications in chemistry, biology, geology, and industry. Biological systems are often crowded aqueous environments filled with proteins, membranes, vesicles, and other structures that often rely on the presence of ions for stability and proper functioning [1–6]. The ion–water interface is critical for ion exchange resins [7, 8], heterogeneous catalysis [9–11], electrochemistry [12], as well as processes involving mineral dissolution [13, 14] and ion adsorption [15, 16]. Because the behavior of water in the presence of ions impacts a wide range of technical and scientific fields, a great deal of literature over the years has been dedicated to studying the aqueous solvation of ions and the properties of water at charged interfaces. Studies that have examined ion–water interfaces have employed *x*-ray and neutron diffraction [17–19], Raman spectroscopy [20], ultrafast infrared spectroscopy [21–26], Fourier transform

Vibrational Spectroscopy at Electrified Interfaces, First Edition.
Edited by Andrzej Wieckowski, Carol Korzeniewski, and Björn Braunschweig.

infrared (FTIR) spectroscopy [20, 27], and other spectroscopic techniques [15, 28, 29]. Theoretical models [30, 31], molecular dynamics (MD) simulations [32–35], and Monte Carlo (MC) calculations [20] have also been employed. While simulations can provide some insight into the underlying dynamics, most experimental techniques only provide steady-state data. Here we utilize ultrafast infrared spectroscopy to examine the hydrogen bonding dynamics of water at several types of charged and uncharged interfaces.

Ultrafast infrared spectroscopy has been shown to be a powerful technique for elucidating dynamics in water–ion systems [21–26], other hydrogen bonding systems [36–43], protein environments [44–52], and systems that undergo chemical exchange [25, 53–57]. Here, we apply ultrafast infrared pump–probe and two-dimensional infrared (2D IR) vibrational echo spectroscopic techniques to examine the dynamics of water when it is confined in nanoscopic environments and interacting with interfaces. The question is whether the nature of confinement or the chemical composition of the interface most significantly influences the dynamics. To explore this question, the dynamics of water at charged and neutral interfaces in reverse micelles are compared. In addition, water in ionic solutions is investigated. Some water molecules are hydrogen bonded to ions, while others are hydrogen bonded to water molecules. These are in equilibrium, with water molecules bound to ions switching and becoming bound to water molecules, and vice versa. Using 2D IR chemical exchange spectroscopy, we determine the exchange time required for a water hydroxyl initially hydrogen bonded to an anion to switch to being hydrogen bonded to another water molecule.

Reverse micelles consist of a water pool surrounded by a layer of surfactant molecules and are often used as model systems for confined environments. The surfactant molecules are terminated by a hydrophilic head group that can be either charged or neutral. These hydrophilic head groups face in toward the water pool while the alkyl (hydrophobic) tails of the surfactant are suspended in a nonpolar organic phase. A schematic of a reverse micelle utilizing the surfactant Aerosol-OT, or AOT [sodium bis(2-ethylhexyl) sulfosuccinate], is shown in Figure 1.1. The AOT surfactant (Fig. 1.2) forms spherical monodispersed reverse micelles that have been well characterized. The size of the AOT reverse micelles can be easily controlled by varying the amounts of starting materials according to the w_0 parameter: $w_0 = [H_2O]/[\text{surfactant}]$ [58–60]. AOT can yield sizes of $w_0 = 0$ (essentially dry reverse micelles) all the way up to $w_0 = 60$, which has a water pool diameter of 28 nm and contains ~350,000 water molecules [61]. Isooctane is a common solvent used as the nonpolar phase of AOT reverse micelle systems, but other solvents such as carbon tetrachloride, cyclohexane, and benzene can also be used with minimal changes in water pool size for a given w_0 [62]. A recent study has shown that the identity of the nonpolar phase has no effect on the water pool dynamics [63].

As shown in Figure 1.2, AOT has a sulfonate head group with a sodium counterion. The head group region of the reverse micelle therefore creates a charged interface that surrounds the water pool. The sodium ions will generally reside in a region close to the interface. Figure 1.1 illustrates the regions of a reverse micelle. When the total water pool diameter, d, is sufficiently large (≥4.6 nm) the reverse

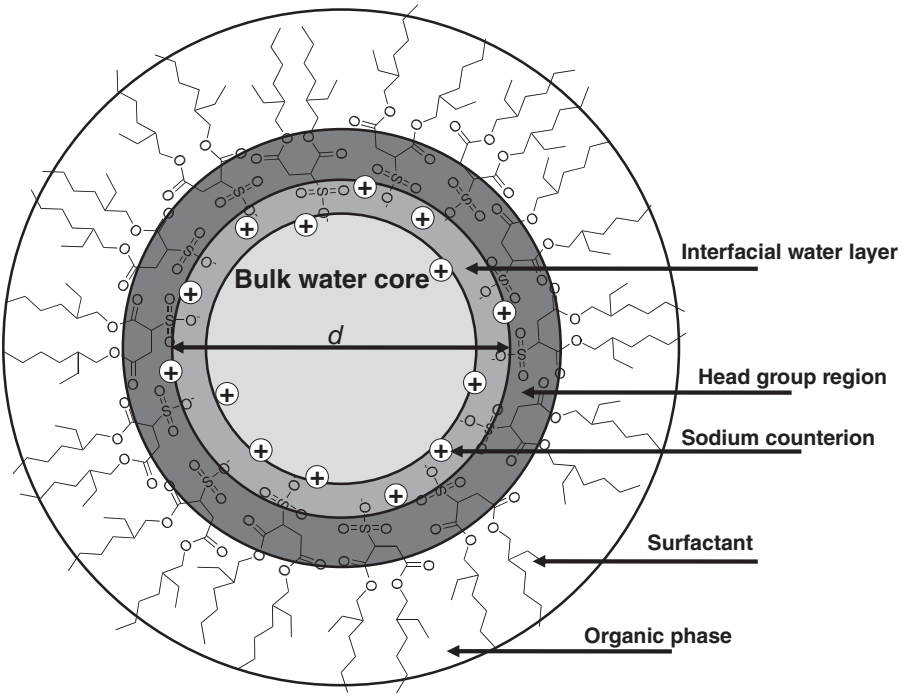

Figure 1.1 Illustration of the reverse micelle interior. The bulk water core is surrounded by a layer of interfacial water. The total water pool diameter is denoted by *d*. The hydrophilic AOT head groups face in toward the water pool while the alkyl tails are suspended in the organic phase. The sodium counterions are dispersed in the water pool, but they generally reside close to the head group interface.

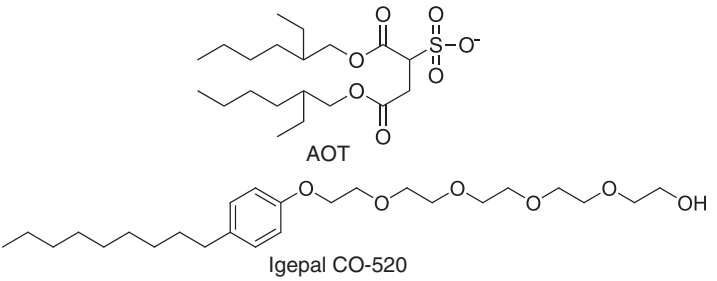

Figure 1.2 Molecular structures for AOT and Igepal CO-520. AOT (top) is terminated by a charged sulfonate head group with a sodium counterion while Igepal (bottom) has a neutral hydroxyl head group.

micelle can support a core of water with bulklike properties. Below we will discuss how far perturbations from the charged sulfonate interfacial region extend into the water pool and what happens to the water dynamics as the size of the water pool changes in size. The chemical identity of the surfactant layer can be changed by using a neutral surfactant molecule called Igepal CO-520 (Fig. 1.2). Igepal is terminated with neutral hydroxyl head groups, so the interfacial water molecules will be exposed to a very different chemical surface compared to the AOT reverse micelle system. To what extent changes in surfactant identity, particularly charged versus neutral head group regions, and reverse micelle size affect water dynamics will be described.

Water dynamics are investigated through the processes of orientational relaxation, spectral diffusion, and vibrational relaxation, which can be measured with ultrafast infrared vibrational spectroscopy. These observables report on how the hydrogen bond network of water evolves and rearranges over time. The hydroxyl stretch of water is monitored during the experiments and is used as a reporter for hydrogen bond dynamics. During vibrational relaxation, vibrational energy dissipates by transferring into a combination of low-frequency modes, such as torsions and bath modes [64, 65]. Energy must be conserved during this process. Certain pathways that facilitate vibrational relaxation in one system may or not be present in a different system. Thus, vibrational relaxation is extremely sensitive to local environments. Orientational relaxation measures how quickly water molecules reorient by monitoring the direction of the transition dipole of the hydroxyl stretch. Molecular reorientation is involved in water hydrogen bond exchange, which leads to global hydrogen bond network reorganization [66, 67]. Bulk water consists of an extended network of hydrogen bonds that are continually rearranging and exchanging with one another. According to the theory of Laage and Hynes, water molecules exchange hydrogen bonds via a jump reorientation mechanism that involves concerted motions of water molecules in the first and second solvation shells [66, 67]. The mechanism proceeds when a molecule in the second solvation shell of another water molecule moves in toward the first solvation shell. In order to swap hydrogen bonds with the approaching water from the second solvation shell, a water molecule must pass through a five-coordinate transition state and then undergo a large-amplitude rotational motion (or "jump"). The jump allows it to switch one of its hydrogen bonds to the approaching water molecule. These large-amplitude jumps change the orientation of the transition dipole. Solutes and interfaces (such as the surfactant shell of the reverse micelles) can disrupt the jump reorientation mechanism, thus slowing down the process of reorientation [23, 68–72]. Both vibrational and orientational relaxation can be measured with ultrafast infrared pump–probe spectroscopy.

Ultrafast 2D IR vibrational echo spectroscopy is used to measure spectral diffusion of the water hydroxyl stretch. The linear infrared absorption spectrum of the hydroxyl stretch is very broad due to a large distribution in the lengths and strengths of hydrogen bonds. At the beginning of the 2D IR experiment, a hydroxyl will vibrate at a certain frequency, but due to dynamic structural evolution of the system, that frequency will change over time. This process of frequency evolution is known

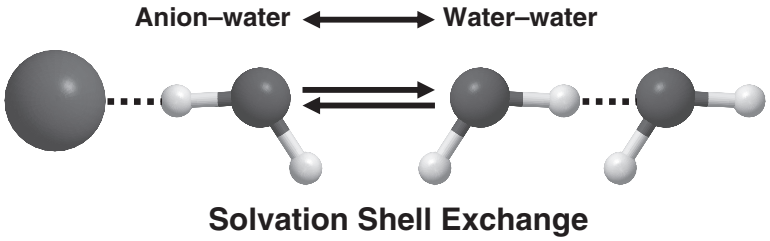

Figure 1.3 Representation of solvation shell exchange. The time it takes for a water hydroxyl initially hydrogen bonded to an anion (left side) to switch to being hydrogen bonded to another water hydroxyl (right side) can be measured with 2D IR vibrational echo spectroscopy.

as spectral diffusion and reports on how quickly water molecules sample different structural environments.

In addition, 2D IR vibrational echo chemical exchange spectroscopy is used to examine how quickly a water hydroxyl bound to an anion will switch to being hydrogen bonded to a neighboring water hydroxyl. This process is illustrated schematically in Figure 1.3. A model system for studying water–ion exchange is a solution of sodium tetrafluoroborate ($NaBF_4$) in water because the linear IR absorption spectrum of the solution yields two resolved peaks corresponding to waters interacting with other waters and waters interacting with the tetrafluoroborate anions. It is found that the ion–water hydrogen bond switching time is ~7 ps [25]. This switching time has implications when treating the orientational relaxation dynamics of water molecules inside reverse micelles made of charged and neutral surfactants [71]. Together, these ultrafast infrared experiments involving water in reverse micelles and water–ion chemical exchange construct a dynamic picture of the behavior of water molecules at charged interfaces and interacting with ions.

1.2 EXPERIMENTAL METHODS

1.2.1 Sample Preparation

Carbon tetrachloride (CCl_4), cyclohexane, isooctane, H_2O, D_2O, AOT, Igepal CO-520, and $NaBF_4$ were used as received. Stock solutions of 0.5 M AOT were prepared in CCl_4, cyclohexane, and isooctane. A variety of solvents are necessary due to certain experimental considerations that will be discussed below. A 0.3-M stock solution of Igepal CO-520 was prepared in cyclohexane. The residual water contents of the stock solutions were measured via Karl Fischer titration. The reverse micelle samples were prepared by mass by adding appropriate amounts of a solution of 5% HOD (water with one hydrogen exchanged with deuterium) in H_2O to measured quantities of the AOT or Igepal stock solutions to obtain the desired w_0. In the ultrafast experiments, the OD stretch of 5% HOD in H_2O is probed because it not only provides an isolated stretching mode to interrogate but also prevents vibrational excitation transfer processes from artificially causing decay of the orientational correlation function and observables related to spectral diffusion [73, 74]. MD simulations demonstrate that

a dilute amount of HOD does not perturb the structure and properties of H_2O and that the OD stretch reports on the dynamics of water [75].

For the pump–probe experiments involving large reverse micelles presented here, the 0.5-M stock solution of AOT in isooctane was used to make samples of $w_0 = 10$, 16.5, 25, 37, and 46 (diameters of 4.0, 5.8, 9, 17, and 20 nm, respectively). It has been found that the combination of AOT and isooctane causes distortions in vibrational echo experiments, so for vibrational echo experiments on small reverse micelles the 0.5-M AOT/CCl_4 stock solution was used to make $w_0 = 2$, 4, and 7.5 (diameters of 1.7, 2.3, and 3.3 nm, respectively) [63]. CCl_4 cannot support reverse micelles larger than $w_0 \sim 10$ [61], so the 0.5-M AOT/cyclohexane stock solution was used to make $w_0 = 12$ and 16.5 (diameters of 4.6 and 5.8 nm, respectively) for vibrational echo experiments on larger reverse micelles. Neither CCl_4 nor cyclohexane cause distortions in the vibrational echo experiments. Cyclohexane can only reliably make reverse micelles of $w_0 < 20$ [76, 77], so the vibrational echo studies are limited to the lower bound of large sizes. It will be shown that both $w_0 = 12$ and 16.5 have well-defined bulk water cores and interfacial water regions, so analysis of these sizes should provide insight into the behaviors of water molecules in the even larger sizes.

To compare the effects of the chemical composition of the interface, Igepal reverse micelles with $w_0 = 12$ and 20 were also made. Like AOT, Igepal also makes monodispersed spherical reverse micelles [78]. The AOT and Igepal surfactants have different aggregation numbers, thus yielding different sizes for the same w_0 values. The $w_0 = 12$ Igepal reverse micelles have the same 5.8-nm diameter as AOT $w_0 = 16.5$ while the $w_0 = 20$ reverse micelles have the same 9-nm diameter as AOT $w_0 = 25$. AOT lamellar structures (sheets of AOT surfactants with water between them) were prepared by adding water to dry AOT to produce samples with various water-to-surfactant ratios, λ. These lamellar samples allow us to examine the effects of confining geometry on the water dynamics (spherical confinement versus confinement within layers).

The experimental samples are contained between two calcium fluoride windows that are separated by a Teflon spacer. The thickness of the Teflon spacer is chosen such that the optical density of the OD stretch region is ~0.1 for the vibrational echo experiments and ~0.5–0.7 for the pump–probe experiments.

For the 2D IR chemical exchange experiments, a 5.5-M solution of $NaBF_4$ in water was used. Again, the water component consisted of 5% HOD in H_2O for the same reasons outlined above. The 5.5-M concentration corresponds to a system with seven water molecules per $NaBF_4$ molecule ($n = 7$). For linear IR absorption measurements, additional samples of 1.7 M, 3.1 M, and 4.3 M of $NaBF_4$ in water were made, corresponding to $n = 30$, 15, and 10, respectively.

1.2.2 2D IR Vibrational Echo Spectroscopy

The laser system used to generate the infrared light that excites the OD hydroxyl stretch consists of a Ti–sapphire oscillator that seeds a regenerative amplifier. The

output of the regenerative amplifier pumps an optical parametric amplifier that generates near-infrared wavelengths that are difference frequency mixed in a $AgGaS_2$ crystal. The resulting mid-IR pulses are centered at ~4 μm (2500 cm^{-1}) but can be tuned to the peak of the absorption spectrum for a given sample (e.g., 2565 cm^{-1} for $w_0 = 2$ AOT reverse micelle). The generated mid-IR beam enters a 2D IR vibrational spectrometer that can be readily converted into a pump–probe setup.

The pump–probe and 2D IR vibrational echo techniques presented here are noncollinear four-wave mixing experiments [79, 80]. In these experiments, three field–matter interactions between the sample and the incident ultrafast laser pulses create a third-order macroscopic polarization that emits a signal electric field. Depending upon the type of experiment, the signal electric field carries different types of information. As discussed in the introduction, the signal from a pump–probe experiment allows one to extract vibrational lifetimes and orientational relaxation parameters for the OD stretch of HOD in H_2O. The vibrational lifetime and orientational observables are sensitive to local structural and chemical environments. 2D IR vibrational echo spectroscopy is a sophisticated technique that observes how vibrational chromophores in a system evolve in frequency over time via chemical exchange, spectral diffusion, coherence transfer, or other processes. 2D IR spectroscopy can monitor these frequency changes by manipulating the quantum pathways by which the system evolves.

The experimental pulse sequence for the 2D IR vibrational echo experiments is shown in Figure 1.4*a*. The pump–probe experiment (Fig. 1.4*b*) is similar in several ways to the 2D IR experiment, but it differs in the number of input beams and the manner by which the signal is detected. In the 2D IR experiment, three time-ordered

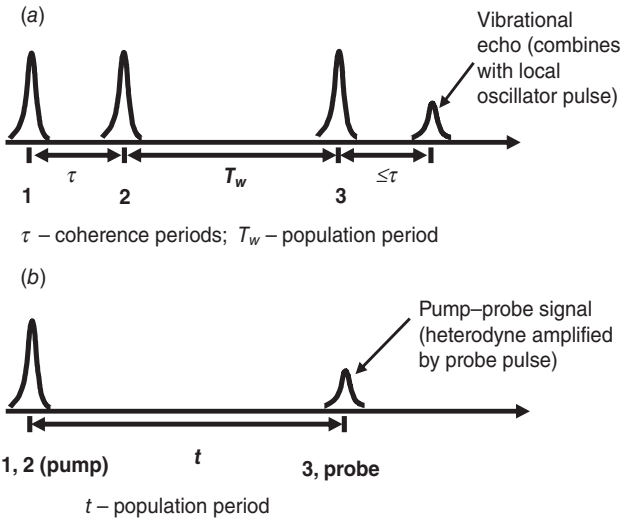

Figure 1.4 Pulse sequences implemented for (*a*) 2D IR vibrational echo spectroscopy and (*b*) pump–probe spectroscopy. Both techniques are noncollinear four-wave mixing experiments.

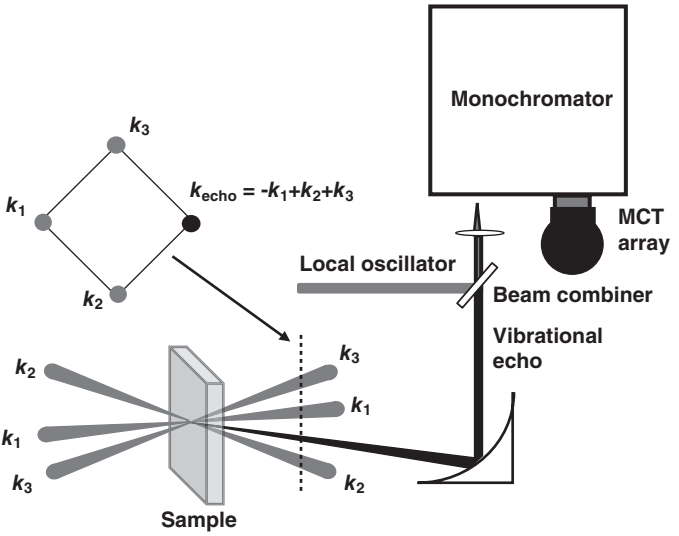

Figure 1.5 Experimental setup for the 2D IR vibrational echo experiment. Three excitation beams in a BOXCARS geometry cross in the sample to produce the vibrational echo signal in the phase-matched direction denoted by the wave vector k_{sig}. The vibrational echo signal combines with a local oscillator beam for heterodyned detection. The heterodyned signal is detected by a 32-pixel MCT array detector.

beams interact with the sample (Fig. 1.5). The first pulse induces a coherence state between the ground (0) and first excited (1) vibrational levels. The vibrations are initially in phase, but inhomogeneous broadening of the absorption line and structural fluctuations cause the phase relationships to decay. After a period of time, τ, a second pulse impinges on the sample and creates a population state in either the 0 or 1 vibrational levels. A time period T_w elapses (the waiting time) before the third pulse reaches the sample and induces a second coherence state, partially restoring the phase relationships between the vibrational chromophores. This rephasing process causes the vibrational echo signal electric field to emit at a time $t \leq \tau$. The vibrational echo signal propagates in the phase-matched direction according to $k_{sig} = -k_1 + k_2 + k_3$, as denoted by the BOXCARS geometry of the input beams shown in Figure 1.5. The vibrational echo signal is temporally and spatially overlapped with a local oscillator (LO) pulse for heterodyned detection. The LO is another IR pulse identical to the excitation pulses but lower in amplitude and fixed in time. The combined vibrational echo and LO beam is frequency dispersed by a monochromator, and the heterodyned signal is detected on a 32-pixel mercury–cadmium–telluride (MCT) array detector. If we denote the vibrational echo signal as S and LO signal as L, then the quantity $|S + L|^2 = S^2 + 2LS + L^2$ is measured on the detector. Assume S^2 is negligible and can be ignored and L^2 is a constant signal and can be subtracted. The $2LS$ cross term represents the heterodyned signal of interest.

Ultimately, the 2D IR experiment obtains frequency correlation plots (2D spectra) for the second coherence period (known as the detection time period) and

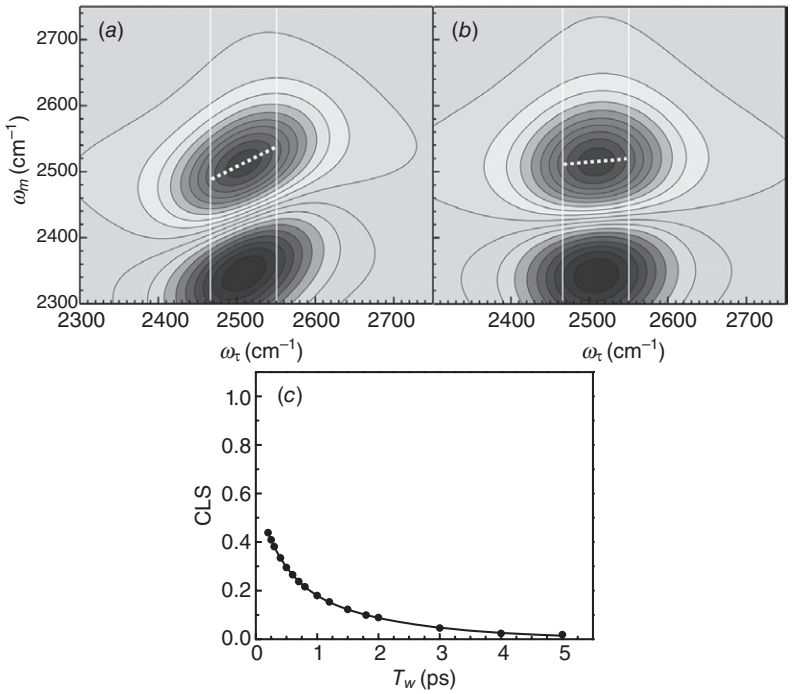

Figure 1.6 CLS procedure: (*a*) bulk water 2D spectrum at $T_w = 0.2$ ps, showing elongation along the diagonal and (*b*) bulk water spectrum at $T_w = 2$ ps. Spectral diffusion has mostly completed, so the spectra become more circular. The white solid lines show the direction of cuts during the CLS procedure. The white dots indicate the peak positions through the slices (centerline data). The slope is found through each set of peak positions at each T_w to obtain a plot of slope versus T_w, as shown in panel (*c*). The CLS curve is equal to the normalized FFCF, which is shown as the black line through the CLS data.

the first coherence period (known as the evolution time period). Each frequency axis of the correlation plot arises from Fourier transformation of each coherence period. The Fourier transform along the second coherence period is performed experimentally by the monochromator, yielding the vertical "ω_m" axis while the Fourier transform along the first coherence period is obtained numerically during data processing, yielding the horizontal "ω_τ" axis. These axes are clearly marked in Figures 1.6*a*, *b*, which show correlation spectra for bulk water (5% HOD in H_2O). During the experiment, τ is scanned for a series of fixed T_w values. As τ is scanned, the echo signal field moves in time relative to the fixed LO. The echo field goes in and out of phase with the LO field producing an interferogram. Mixing the vibrational echo signal with the LO allows interferograms to be recorded, thus providing the necessary phase information for Fourier transformation.

Qualitatively, a 2D IR vibrational echo experiment works in the following manner. The first laser pulse "labels" the initial structures of the species by establishing their initial frequencies, ω_τ. The second pulse ends the first time period τ and

starts the reaction time period T_w during which the labeled species undergo structural evolution. For example, the local hydrogen bond network rearranges. This ends the population period of length T_w and begins a third period of length $\leq\tau$, which ends with the emission of the vibrational echo pulse of frequency ω_m, which is the signal in the experiment. The vibrational echo signal reads out information about the final structures of all labeled species by their frequencies, ω_m. During the period T_w between pulses 2 and 3, the system's structural evolution occurs. The structural evolution and associated frequency changes as T_w is increased cause new off-diagonal peaks to grow in a chemical exchange experiment or the shape of the 2D spectrum to change in a spectral diffusion experiment. The growth of the off-diagonal peaks or the change in the 2D band shapes in the 2D IR spectra with increasing T_w provides the dynamical information.

The 2D IR experiments require precise timing between the excitation pulses as well as phase stability during the coherence periods. Computer-controlled precision delay lines (Aerotech ANT-50L) manipulate the delay between the excitation pulses, and a three-pulse cross-correlation measurement is used to check the timing and correct for drifts between the three excitation pulses [63]. The vibrational echo experiments are also sensitive to linear chirp in the mid-IR pulse. Linear chirp is corrected by proper insertion of materials (calcium fluoride and germanium) with opposite signs of the group velocity dispersion (GVD) [82, 83].

The 2D IR experiments presented here are used to determine the frequency–frequency correlation function (FFCF) of water molecules (OD stretch), which is a measure of spectral diffusion. The FFCF can be determined via the centerline slope (CLS) method [84, 85]. Figure 1.6 illustrates this process. In the CLS technique, the 2D IR spectrum is sliced parallel to the vertical ω_m axis over a range of frequencies surrounding the center of the 2D IR spectrum. In Figures 1.6*a*,*b*, the solid white lines show the direction of slicing and the bounds over which the slices are taken. For water systems (as shown in the figure), the range is typically $\pm$30–40 cm^{-1} around the measured center frequency of each 2D IR spectrum. Each slice intercepts a frequency on the horizontal ω_τ axis. The slices are fit to Gaussian line shape functions to determine the peak position of each slice. Only the peak positions are required. The peak positions (white dots) are plotted versus their corresponding ω_τ frequencies, and the slope of the resulting line is calculated. This process is repeated for all T_w values so that a plot of slope versus T_w is obtained (Fig. 1.6*c*). Generally, the 2D plots show elongated spectra at early T_w, as shown by Figure 1.6*a*. By 2 ps (Fig. 1.6*b*), the spectra show a more circular shape because most of the water hydroxyl environments in the H_2O inhomogeneous line shape have been sampled by the OD vibrational chromophore, indicating that spectral diffusion is nearly complete.

It has been demonstrated theoretically that the CLS curve of slope versus T_w is equal to the T_w-dependent portion of the normalized FFCF [84, 85]. The FFCF adopts a functional form that contains both homogeneous (motionally narrowed) and inhomogeneous components,

$$C_1(t) = \langle \delta\omega_{10}(t)\delta\omega_{10}(0)\rangle = \frac{\delta(t)}{T_2^*} + \sum_i \Delta_i^2 e^{-t/\tau_i} \tag{1.1}$$